Lisbon School of Economics & Management
Universidade de Lisboa

MASTER OF SCIENCE

MATHEMATICAL FINANCE

MASTER'S FINAL WORK

DISSERTATION

PRICING RENEWABLE ENERGY CERTIFICATES

VASCO CAPELA TAVARES

OCTOBER-2023

Lisbon School of Economics & Management
Universidade de Lisboa

MASTER OF SCIENCE

MATHEMATICAL FINANCE

MASTER'S FINAL WORK

DISSERTATION

PRICING RENEWABLE ENERGY CERTIFICATES

VASCO CAPELA TAVARES

SUPERVISOR:

JOÃO MIGUEL ESPIGUINHA GUERRA

OCTOBER-2023

Abstract

This thesis is concerned with a pricing model of renewable energy certificates. We study a stochastic model based on a system of forward-backward stochastic differential equations with two stochastic factors. The forward processes are the accumulated renewable energy certificates and the renewable energy production rate, while the backward process is the certificate's price. This setting allows us to derive a non-linear partial differential equation for the price. The first step in finding a numerical solution for that equation is its linearization via a duality algorithm. To solve the obtained linearized problem, we then use a characteristics scheme in time with finite differences discretization. Finally, the convergence of the algorithm is checked, alongside its application to a real world problem and an analysis of the equation's sensitivity to its parameters.

Keywords: Renewable Energy Certificates; Forward Backward Stochastic Differential Equations; Non-Linear Partial Differential Equations; Characteristics Scheme; Environmental Quantitative Finance.

JEL Codes: C60; C61; C63; C65; C69.

Acknowledgements

This thesis is not only a result of my academic path but also a by-product of my life's journey so far. It is impossible to encompass my gratitude to all the people who have positively influenced my life, but this is my best effort to do so.

First and foremost, I thank my supervisor, Professor João Guerra, for his help and guidance throughout this thesis and previous courses where he was my professor. Apart from his relevant contributions to this work, I remember our frequent meetings never had a scheduled ending time, they lasted for as long as I needed to. This says everything about Professor João's support, patience, and good, approachable character. Thank you for making this difficult process easier than it could have been.

I extend this gratitude to my family. To my mother Sónia for her unconditional love, support, and encouragement; to my father Fernando; to my grandparents Antenor and Maria Isabel for their unwavering presence, confidence in me, and for being my role models concerning resilience and positivity; to my godparents Vanda and Vitó for their proximity and affability; and to my cousins Diogo and Marta for all the great childhood memories and for their friendship.

I am also immensely grateful to Estela for her constant love, patience, care, and good humour. Thank you for being with me through all the years, you really are my favourite swiftie mathematician. I also thank two of my closest friends: Tiago Lourenço for his unchangeable companionship and different views, and Tiago Teixeira for being by my side through the hard Physics days and in this elegant fall into the unmagnificent lives of adults.

Lastly, a note to self. Let this thesis be part of a meaningful life aimed at being a force of good and positivity in the world. "Soak it in for the rain will pass in time, nothing wrong in sinking low, you're the omen of paradise".

List of Acronyms

ACP	Alternative Compliance Payment
EMM	Equivalent Martingale Measure
ETS	Emissions Trading Scheme
EU	European Union
FBSDE	Forward-Backward Stochastic Differential Equation
GC	Green Certificate
LSE	Load-Serving Entity
ODE	Ordinary Differential Equation
OECD	Organization for Economic Cooperation and Development
OU	Ornstein-Uhlenbeck
PDE	Partial Differential Equation
REC	Renewable Energy Certificate
SDE	Stochastic Differential Equation
SREC	Solar Renewable Energy Certificate
USA	United States of America

Contents

Chapter 1

Introduction

Last year, the globe watched unprecedented news: we are now more than 8 billion (United Nations, 2022). The developments of mankind over the past decades have been unparalleled, and that is not just measured by population size. According to the World Bank, approximately 1.4 billion people have been lifted out of the $2.15 per day poverty line in the past three decades (World Bank, 2023).

As an immediate result, energy consumption has risen across the world. On the supply side, the International Energy Agency estimated in 2021 that the world's main energy source is oil, as it composes more than 30% of the global share of total energy supply. Coal and natural gas are the close second and third on the list, respectively. Renewable energy accounts to less than 15% of the current energy supply, and OECD countries' efforts to cut back on the usage of coal have been outweighed by a heavily coal-dependent China. However, there is a general trend to adopt renewable sources of energy with the production of, for example, hydroelectricity, wind electricity, and solar photovoltaic electricity (International Energy Agency, 2021).

The problem with non-renewable energy exceeds its inevitable end; it is also pollutant. Since the Industrial Revolution, as a by-product of the aforementioned economic success, the concentrations of greenhouse gases have increased due to human activities. Because of the implications of global warming, world leaders came together and, in 1997, the Kyoto Protocol was adopted. The main objective of the Kyoto Protocol was to address climate change by reducing the emission of greenhouse gases that contribute to global warming. It was initially signed by 192 countries, but the United States (USA), the world's largest emitter of greenhouse gases, never ratified the agreement. Canada withdrew from the protocol in 2012, and Russia, Japan, and New Zealand did not participate in the second commitment period. Nevertheless, the agreement estab-

lished a carbon trading system that allows countries that have exceeded their targets to purchase emissions credits from other countries that have reduced their emissions below their targets (United Nations, 1997).

To comply with this goal, the European Union (EU) established an Emissions Trading System (ETS) in 2005. It has led to emission reductions and increases in clean innovation without losing competitiveness and thus carbon markets were implemented worldwide (Chassagneux et al., 2017). Over the past decade, pricing mechanisms of carbon permits have been studied. Namely, Forward-Backward Stochastic Differential Equations (FBSDEs) are introduced in pricing models in Carmona et al. (2012); a similar model is used in Howison and Schwarz (2012) and the focus is on the Partial Differential Equation (PDE) representation.

Another relevant tool to implement green policies is the use of Renewable Energy Certificates (RECs), often called Green Certificates (GCs) in Europe. These are especially useful in the USA, where there is no national carbon market. Nevertheless, REC markets are also emerging in Europe due to the challenges that arise from an oversupplied European carbon market, and are well established in Australia and India (Coulon et al., 2015). Instead of a cap-and-trade system such as the EU ETS, RECs provide a market-based alternative. When renewable energy generators fulfil specific criteria, they obtain a REC for a designated unit, usually 1 MWh of renewable electricity generated. This REC can be sold to a Load-Serving Entity (LSE) that must meet an annual target for procuring a certain percentage of renewable electricity. If that entity fails to fulfil this quota, they incur a penalty known as the Alternative Compliance Payment (ACP) (Baamonde-Seoane et al., 2021). In this way, RECs can be quite useful in the companies' investment strategies. On one hand, buyers can cover their requirements of generating green energy by purchasing RECs instead of making a big investment to produce green energy themselves; on the other hand, sellers can finance their renewable energy installations by selling RECs (Baamonde-Seoane et al., 2021).

Academic studies on REC markets are more recent than research on cap-and-trade systems for carbon markets (Coulon et al., 2015). While there are similarities, carbon and REC markets exhibit some differences, namely on the source of uncertainty and the regulator's stipulations. In REC markets, uncertainty comes from the certificate supply driven by energy generation processes whereas in carbon markets it arises from allowance demand. Besides that, in the former case the regulator determines demand (requirement) rather than supply (cap) (Baamonde-Seoane et al., 2021).

In this thesis, we assume that the price of these certificates depends on two stochastic factors: the accumulated RECs and the renewable energy production rate. So, a coupled system of FBSDEs to value RECs is proposed and the associated PDE is derived. As it will be shown, the PDE we derive is a convection-diffusion equation, which are widely used in Mathematical Finance as they model, for instance, the behaviour of one-factor option pricing problems (Duffy, 2006). However, the PDE shows some intricacies, as it is nonlinear (more precisely, semilinear) and degenerate.

The PDE's non-linearity will be tackled following the work by Baamonde-Seoane et al. (2021). The semilinear term is written in terms of a maximal monotone operator that introduces a nonlinear system which is solved by a fixed point iteration.

To address the fact that the PDE is degenerate, we also follow the work of Baamonde-Seoane et al. (2021) and consider it as a limit case of a convection-dominated problem. These problems are common in fluid dynamics applications and impact the stability of numerical schemes. A good review of convection-dominated problems can be found in the review article by Cockburn and Shu (2001). The authors highlight that finite difference methods are only first-order accurate when the solution is smooth and generate spurious oscillations around the discontinuities which impact in a non-trivial way the convergence of the method due to the non-linear nature of the equation. The inaccuracy of finite difference methods in convection-dominated problems is also mentioned in Duffy (2006). To overcome such difficulties, we will use a semi-Lagrangian numerical scheme proposed by Baamonde-Seoane et al. (2021), which is especially suited for convection-dominated problems.

To achieve the goals here proposed, this thesis is structured as follows: after this introduction, Chapter 2 presents the stochastic model for RECs pricing. The numerical method to solve the PDE that arises from that model is presented in Chapter 3, whose results are shown in Chapter 4. In the fourth chapter we will also perform a sensitivity analysis of the parameters in the model that have a real-world interpretation. Lastly, we summarize the results.

Chapter 2

A Framework to Model the Price of Renewable Energy Certificates

In this Chapter, we introduce the mathematical framework and the stochastic models that allow us to price RECs. First, we mathematically define the market in which we will operate. We also see how regulatory measures enable a clear determination of the certificate's price at compliance date. Secondly, we demonstrate how the arbitrage-free price of a REC appears as the solution to a PDE, after following the approach of using a coupled system of FBSDEs.

2.1 Market Setup

We consider a finite time horizon $[t_0, T]$, where $T \in [t_0, \infty)$. To simplify our initial setup, we identify T as the single compliance date, but we later introduce multiple compliance periods. Following the setting of Schwarz (2012), let $(\Omega, \mathcal{F}, (\mathcal{F}_t)_{t\in[t_0,T]}, \mathbb{P})$ be a filtered probability space satisfying all the usual assumptions. Note that $(\mathcal{F}_t)_{t\in[t_0,T]}$ is generated by a standard Brownian motion $(W_t)_{t\in[t_0,T]}$ and $\mathbb{P}$ is the real-world measure. We also work under the principle of no arbitrage. Then, by the First Fundamental Theorem of Asset Pricing (see, for example, Björk (2020, chap. 11)), there exists a equivalent martingale measure (EMM) $\mathbb{Q}$. Then, it is a matter of choosing the appropriate EMM (we refer the reader to Cont and Tankov (2003) for a detailed explanation). However, the local mean rate of return of any derivative price process is the risk-free interest rate under a EMM, which is our foremost concern.

2.2 Derivation of a Pricing Equation

To model the price of a REC we assume it is a stochastic process, which is denoted at time t by P_t. Following the work of Baamonde-Seoane et al. (2021), we assume it depends on two stochastic factors whose values are known at an initial time t_0: the renewable energy generation rate and the accumulated number of certificates, denoted by G_t and B_t, respectively.

The renewable energy generation rate is mainly driven by weather patterns and the construction of new infrastructure. Moreover, the basic and classical model for temperature dynamics is the Ornstein-Uhlenbeck (OU) model (Benth et al., 2008). This is basically a mean-reverting autoregressive model with lag 1 in continuous time. The exponential of an OU process is also the classical stochastic model for the spot dynamics of commodity prices, introduced by Schwartz (1997). The fact that it is a mean-reverting and strictly positive process makes it a good candidate to model the renewable energy generation rate. So, we take $G_t = \exp\left(\tilde{G}_t\right)$, where $\tilde{G}_t$ is an OU process that satisfies the following forward SDE:

$$\tilde{G}_t = g_0 + \int_{t_0}^{t} \alpha_g \left(f(s) + \frac{\beta_g}{\alpha_g} P_s - \tilde{G}_s \right) \mathrm{d}s + \int_{t_0}^{t} \sigma_g \, \mathrm{d}W_s^0, \quad \text{for } t \in [t_0, T]. \tag{2.1}$$

Note that W_t^0 is a standard $\mathcal{F}_t$-adapted $\mathbb{Q}$-Brownian motion and $g_0 \in \mathbb{R}$. Moreover, we take a constant volatility σ_g and the drift features a mean reversion speed α_g and a parameter, β_g, that controls the feedback from the REC price. It captures the tendency to install new renewable energy production infrastructure when REC prices are high. This is an immediate feedback, as discussed and compared with lagged feedbacks in Coulon et al. (2015). The authors argue that although a lagged feedback is more reasonable since building the aforementioned infrastructure takes time, an immediate feedback preserves the main features of the model and simplifies computations.

The drift also includes a deterministic function f, which is a linear combination of sine and cosine functions to represent the influence of weather on REC prices. The idea of a deterministic function to add seasonality that represents the influence of weather conditions to the model is also considered in Coulon et al. (2015). It has the following form:

$$f(t) = a_1 \sin(4\pi t) + a_2 \cos(4\pi t) + a_3 \sin(2\pi t) + a_4 \cos(2\pi t), \tag{2.2}$$

where the coefficients $a_i \in \mathbb{R}, i \in \{1, 2, 3, 4\}$. This will be the function that is incorporated into our model.

As for the accumulated number of RECs, it is simply the sum in continuous time of the renewable energy generation rate:

$$B_t = \int_{t_0}^{t} G_s \, \mathrm{d}s \,, \quad \text{for } t \in [t_0, T]. \tag{2.3}$$

Since accumulation is measured from the start of the compliance period, we have $B_{t_0} = 0$. Moreover, B_t is a non-decreasing process, which makes sense intuitively because it is a cumulative quantity.

2.2.1 Single Compliance Period

From a financial point of view, it is clear that in a one-period market the value of the certificate at the time of compliance can only take two values: in case the entity fails to comply with the requirements, the certificate price is equal to the ACP; otherwise, in the event of compliance, it is equal to zero. Let π_T be the ACP at compliance time. Therefore,

$$P_T := \psi(B_T) = \pi_T \mathbb{1}_{[0,R_T)}(B_T). \tag{2.4}$$

Under the principle of no arbitrage, the discounted REC price is a martingale under a risk-neutral measure $\mathbb{Q}$. As mentioned before, that measure exists but it is not necessarily unique because we do not assume the market is complete to keep it as general as possible. However, the local mean rate of return of the REC price process is the risk-free interest rate under a EMM. Therefore, we choose a measure $\mathbb{Q}$ that checks this condition, and the price of the certificate at time t is uniquely determined by discounting the conditional expectation of its terminal value (see, for example, Björk (2020)). Thus, for $t \in [t_0, T]$ and considering a constant risk-free interest rate r,

$$P_t = \mathrm{e}^{-r(T-t)} \mathbb{E}^{\mathbb{Q}} \left[\psi(B_T) \mid \mathcal{F}_t \right]. \tag{2.5}$$

After this step, we make use of the Martingale Representation Theorem to get the following expression for the price process:

$$P_t = \pi_T \mathbb{1}_{[0,R_T)}(B_T) - r \int_t^T P_s \, \mathrm{d}s - \int_t^T Z_s^0 \, \mathrm{d}W_s^0 \,, \tag{2.6}$$

where Z_t^0 is some unique, $\mathcal{F}_t$-adapted and square integrable process. We refer the reader to the Appendix for the details of this derivation.

Recalling equations (2.1), (2.3), and (2.6), we conclude that the REC pricing problem consists on the following system of FBSDEs for $t \in [t_0, T]$, written in differential form:

$$\begin{cases} \mathrm{d}\widetilde{G}_t = \alpha_g \left(f(t) + \frac{\beta_g}{\alpha_g} P_t - \tilde{G}_t \right) \mathrm{d}t + \sigma_g \, \mathrm{d}W_t^0 \,, & \widetilde{G}_{t_0} = g_0, \\ \mathrm{d}B_t = \exp\left(\widetilde{G}_t\right) \mathrm{d}t \,, & B_{t_0} = 0, \\ \mathrm{d}P_t = r P_t \, \mathrm{d}t + Z_t^0 \, \mathrm{d}W_t^0 \,, & P_T = \pi_T \mathbb{1}_{[0, R_T)} \left(B_T \right). \end{cases} \tag{2.7}$$

This system of equations resembles those considered to price carbon emission allowances in Howison and Schwarz (2012), Schwarz (2012), and Bento (2022). We highlight that the result of existence and uniqueness of a solution presented in Schwarz (2012) is extended in Bento (2022) for cases where the drift coefficient of the first forward SDE depends explicitly on time, which is the case in (2.7). However, the system in (2.7) is more complex, as the first forward SDE is coupled with the backward SDE, which is not the case in the equations considered to price carbon allowances by the aforementioned authors. Therefore, it is not trivial to use the ideas in Bento (2022) to arrive at a similar result for our system of FBSDEs.

Nevertheless, we assume that a solution for (2.7) exists, as in Baamonde-Seoane et al. (2021). Following the authors' computations (which are fully undertaken and explained in the Appendix), we arrive at the PDE for the price function $P = P(t, B, \widetilde{G})$ associated to the system in (2.7):

$$\mathcal{L}_1[P] = \left[\frac{\partial}{\partial t} + \frac{1}{2} \sigma_g^2 \frac{\partial^2}{\partial \widetilde{G}^2} + \alpha_g \left(f(t) + \frac{\beta_g}{\alpha_g} P - \tilde{G} \right) \frac{\partial}{\partial \widetilde{G}} + \exp\left(\widetilde{G}\right) \frac{\partial}{\partial B} - r \right] P = 0. \tag{2.8}$$

Recalling that the REC value at maturity is given by (2.4) in a single compliance period, then we can define a final value problem joining the previous PDE with the terminal condition

$$P(T, B_T, \widetilde{G}_T) = \pi_T \mathbb{1}_{[0, R_T)}(B_T). \tag{2.9}$$

2.2.2 Multiple Compliance Periods

The results presented in the previous subsection can be extended to an arbitrary number of periods, as in Baamonde-Seoane et al. (2021) and in Schwarz (2012). To address this case, let γ be the number of life years of the REC, i.e., the number of years since it was issued for which it is still valid to be considered for compliance.

At maturity T, the price of the certificate is still equal to the payoff defined in (2.4). However, at each compliance date $T_i, i = 1, \ldots, \gamma - 1$, we must impose a jump condition. At compliance date, the LSE either does not have a sufficient number of RECs and incurs in an ACP, or the number of RECs is greater than the requirement and the LSE uses them.

Let R_i and π_i be, respectively, the requirement and the ACP at time T_i. Moreover, let T_i^+ be the time instant immediately after T_i. The REC value at the compliance date $T_i, i = 1, \ldots, \gamma - 1$ is

$$P(T_i, B, \widetilde{G}) = \max \left[\pi_i \mathbb{1}_{[0,R_i)}(B), P\left(T_i^+, \max(B - R_i, 0), \widetilde{G}\right) \right]. \tag{2.10}$$

Notice that equations (2.8) and (2.10) define a sequence of linked final value problems that is solved for each $i = \gamma - 1, \ldots, 1$.

Chapter 3

Numerical Method

In the previous Chapter, we have posed the final value problems to price RECs according to our model in both the single and multiple period cases. Since there are no analytical solutions for these problems, in this Chapter we revamp the numerical scheme and algorithm presented in Baamonde-Seoane et al. (2021) to approximate them.

First, notice that the natural domain to define the PDE (2.8) is $(t_0, T) \times \mathbb{R}^+ \times \mathbb{R}$. However, the numerical solution requires a bounded domain, so it must be truncated. Moreover, the boundaries must be chosen in a way that the solution's accuracy is not affected in a region of financial interest. This is a common approach in option pricing problems and known as introducing a "far-field condition" (Duffy, 2006). In this Chapter, we establish the boundaries of the truncated domain and impose appropriate conditions at those spatial boundaries.

Secondly, we highlight the intricacies of the PDE (2.8). It is semilinear because the coefficient of the first order derivative with respect to $\widetilde{G}$ depends on P (the dependent variable), and it is also degenerate. To address the nonlinear term, in Baamonde-Seoane et al. (2021) the authors write it in terms of a maximal monotone operator and then apply a duality method. As for the degeneracy of the PDE (2.8), we think of it as a limit case of a convection-dominated problem. This makes it suitable to apply a semi-Lagrangian numerical scheme, where we simultaneously discretize the terms of the first order derivatives with respect to time and to B. Together with a Crank-Nicolson scheme, this method will result in a system of equations that must be solved at each time step. Therefore, a fixed point algorithm to tackle the resulting system is also presented in this Chapter.

3.1 Treating the Nonlinear Convective Term

In Baamonde-Seoane et al. (2021), the authors treat the nonlinear convective term with the Bermúdez-Moreno algorithm (see Bermúdez and Moreno (1981)), which performs a Yosida regularization of a maximal monotone operator.

This technique was also used in Arregui et al. (2005), but the nonlinear term is on the diffusion part. We introduce the maximal monotone operator:

$$m(P) = \begin{cases} 0, & \text{if } P < 0, \\ P^2, & \text{if } P \geq 0. \end{cases} \tag{3.1}$$

So, we can write the PDE (2.8) in terms of the maximal monotone operator (Baamonde-Seoane et al., 2021):

$$\frac{\partial P}{\partial t} + \frac{\sigma_g^2}{2}\frac{\partial^2 P}{\partial \widetilde{G}^2} + \alpha_g\left(f(t) - \widetilde{G}\right)\frac{\partial P}{\partial \widetilde{G}} + \frac{\beta_g}{2}\frac{\partial m(P)}{\partial \widetilde{G}} + \exp\left(\widetilde{G}\right)\frac{\partial P}{\partial B} - rP = 0. \tag{3.2}$$

We also introduce θ, an additional unknown, based on the duality technique developed in Bermúdez and Moreno (1981):

$$\theta = (m - \omega I)(P), \tag{3.3}$$

where $\omega \in \mathbb{R}^+$ is a constant parameter and I is the identity operator.

Let λ be another parameter such that $\lambda\omega < 1$. The Yosida approximation m_λ^ω of the operator $m_\omega = m - \omega I$ appears by using the Bermúdez-Moreno lemma from Bermúdez and Moreno (1981), as we can get the equivalence

$$\theta = (m - \omega I)(P) \iff \theta = m_\lambda^\omega(P + \lambda\theta). \tag{3.4}$$

As for the choice of the parameter λ, the optimal choice for convergence with the same nonlinear term but in the diffusion part was found in Arregui et al. (2008) to be given by $\lambda = 1/2\omega$. With this choice, the Yosida approximation can be computed (Arregui et al., 2005):

$$m_\lambda^\omega\left(P + \frac{\theta}{2\omega}\right) = \begin{cases} -\theta - 2\omega P, & \text{if } P + \theta/2\omega \leq 0, \\ \theta + 2\omega P + \omega^2 - \omega\sqrt{4\theta + 8\omega P + \omega^2}, & \text{if } P + \theta/2\omega \geq 0. \end{cases} \tag{3.5}$$

Now, we introduce the *linear* differential operator

$$\mathcal{L}_2[P] = \left[\frac{\partial}{\partial t} + \frac{\sigma_g^2}{2}\frac{\partial^2}{\partial \widetilde{G}^2} + \alpha_g\left(f(t) - \widetilde{G}\right)\frac{\partial}{\partial \widetilde{G}} + \frac{\beta_g \omega}{2}\frac{\partial}{\partial \widetilde{G}} + \exp\left(\widetilde{G}\right)\frac{\partial}{\partial B} - r\right] P \quad (3.6)$$

and see that we can write (3.2) in an equivalent form (Baamonde-Seoane et al., 2021):

$$\mathcal{L}_2[P] = -\frac{\beta_g}{2}\frac{\partial \theta}{\partial \widetilde{G}}. \quad (3.7)$$

Recalling the equivalence stated in (3.4), the PDE (3.7) is coupled with the nonlinear equation

$$\theta = m_\lambda^\omega(P + \lambda\theta). \quad (3.8)$$

Clearly, equations (3.7) and (3.8) constitute a nonlinear system. As we mentioned before, we will solve it following the work of Baamonde-Seoane et al. (2021) by using a fixed point iteration, which we will describe in a forthcoming subchapter after discretizing the problem.

3.2 Domain Truncation and Boundary Conditions

As we mentioned before, we must consider a bounded domain in order to apply a numerical scheme to solve the PDE (2.8) with the terminal conditions presented in the previous Chapter.

Recalling that γ is the number of life years of the REC, we can rewrite the initial domain of the PDE (2.8) as $\bar{\Omega}^* = (T-\gamma, T)\times\mathbb{R}^+\times\mathbb{R}$. Now, let $\hat{b}$, $\bar{g} \in \mathbb{R}$ be large enough numbers and consider the truncated bounded domain $\bar{\Omega} = (T-\gamma, T)\times(0, \hat{b})\times(-\bar{g}, \bar{g})$. We further introduce the change of variables

$$\hat{B} = \frac{B}{\hat{b}}, \quad \hat{G} = \frac{\widetilde{G} + \bar{g}}{\hat{g}}, \quad (3.9)$$

with $\hat{g} = 2\bar{g}$. Under the new variables $(t, \hat{B}, \hat{G})$, we finally have the truncated domain $\Omega^* = (T-\gamma, T)\times(0,1)\times(0,1)$ where we will apply a numerical scheme.

This change of variables clearly impacts the way the PDE (3.7) is written. To see this, we introduce a more convenient notation for the variables:

$$y_0 = t, \quad y_1 = \hat{B}, \quad y_2 = \hat{G}, \quad (3.10)$$

and define the following sets:

$$\begin{aligned}
&\Omega^* = \prod_{i=0}^{2} \left(\underline{y_i}, \bar{y_i}\right), \quad \Gamma^* = \partial\Omega^*, \\
&\Gamma_i^{*,-} = \left\{y \in \Gamma^* : y_i = \underline{y_i}\right\}, \quad \Gamma_i^{*,+} = \left\{y \in \Gamma^* : y_i = \bar{y_i}\right\}, \quad i = 0, 1, 2.
\end{aligned} \tag{3.11}$$

The operator presented in (3.6) can be rewritten in the following form (please check the Appendix for the details of the derivation):

$$\mathcal{L}_2[P] = \sum_{i,j=0}^{2} a_{ij} \frac{\partial^2 P}{\partial y_i \partial y_j} + \sum_{i=0}^{2} b_i \frac{\partial P}{\partial y_i} - rP, \quad \text{in } \Omega^*, \tag{3.12}$$

where

$$A = (a_{ij}) = \begin{pmatrix} 0 & 0 & 0 \\ 0 & 0 & 0 \\ 0 & 0 & \frac{\sigma_g^2}{2\hat{g}^2} \end{pmatrix},$$

$$\vec{b} = (b_i) = \begin{pmatrix} 1 \\ \frac{1}{\hat{b}} \exp\left(y_2\hat{g} - \bar{g}\right) \\ \frac{\alpha_g}{\hat{g}} \left(f\left(y_0\right) - \left(y_2\hat{g} - \bar{g}\right) + \frac{\beta_g \omega}{2\alpha_g}\right) \end{pmatrix}.$$

Following the work of Baamonde-Seoane et al. (2021) and Oleĭnik and Radkevič (1973), we impose Neumann boundary conditions at the following spatial boundaries:

$$\begin{aligned}
&\frac{\partial P}{\partial y_1} = 0, \quad \text{on } \Gamma_1^{*,+}, \\
&\frac{\partial P}{\partial y_2} = 0, \quad \text{on } \Gamma_2^{*,-} \cup \Gamma_2^{*,+},
\end{aligned} \tag{3.13}$$

as well as the final condition as in (2.9) at the boundary $y_0 = T$ in the single period case. In the multiple period case, the condition (2.10) is analogously applied but at the time boundaries $y_0 = T_i$.

3.3 Defining the Numerical Method

As mentioned before, here we revisit the numerical method introduced in Baamonde-Seoane et al. (2021). The first step is to appropriately discretize the PDE (3.7). We will do so at the same time as we introduce the numerical scheme because the reasoning behind the proposed discretization becomes very intuitive. Then, we devote our attention to the numerical solution of the system defined by (3.7) and (3.8).

3.3.1 Domain Discretization and Finite Differences Scheme

We focus on the linear differential operator (3.6) that is used in (3.7) to define the pricing PDE. That operator is degenerate and to choose an appropriate discretization scheme, we consider it as a limit case of a convection-dominated problem. These are covered, for example, in Douglas and Russell (1982). In this paper, the authors combine finite difference methods with the method of characteristics to address convection-dominated PDEs. We will apply that idea to our case.

We start by considering a change of the time variable: $\tau = T - t$. This way, τ represents the time to compliance date and the PDE (3.7) is defined equivalently in the domain $\widetilde{\Omega} = (0, \gamma) \times (0, 1) \times (0, 1)$.

Then, we revisit the so-called upwind method. It is used in fluid mechanics for equations similar to (3.7), that is, with diffusive and convective terms and dependent on time, and utilized in an option pricing context in Vázquez (1998). According to the author, the departure point of this method is the concept of total derivative, which is here defined by:

$$\frac{DP}{D\tau} = \frac{\partial P}{\partial \tau} - \frac{1}{\hat{b}} \exp\Big(\hat{G}\hat{g} - \bar{g}\Big) \frac{\partial P}{\partial \hat{B}}. \tag{3.14}$$

It represents the total (or material) derivative in the direction $\hat{B}$ associated to the one-dimensional velocity field

$$v = -\frac{1}{\hat{b}} \exp\Big(\hat{G}\hat{g} - \bar{g}\Big),$$

which does not depend on $\hat{B}$ but clearly depends on $\hat{G}$.

With the total derivative defined, we notice that we can group the remaining terms in the PDE (3.7) and define another differential operator in terms of the variables $\hat{B}$ and $\hat{G}$, using the $\mathcal{L}_2$ operator in the form (3.12):

$$\mathcal{A}P = \frac{\sigma_g^2}{2\hat{g}^2} \frac{\partial^2 P}{\partial \hat{G}^2} + \frac{\alpha_g}{\hat{g}} \left(f(T - \tau) - (\hat{G}\hat{g} - \bar{g}) + \frac{\beta_g \omega}{2\alpha_g} \right) \frac{\partial P}{\partial \hat{G}} + \frac{\beta_g}{2\hat{g}} \frac{\partial \theta}{\partial \hat{G}} - rP. \tag{3.15}$$

That way, in this set of variables and in the domain $\widetilde{\Omega}$, the pricing PDE (3.7) is equivalently represented as

$$\frac{DP}{D\tau} - \mathcal{A}P = 0. \tag{3.16}$$

While the total derivative is in the direction $\hat{B}$, the differential operator $\mathcal{A}$ is in the direction $\hat{G}$. It contains convective, diffusive, and reactive terms; in fact, the diffusive and reactive terms are similar to those that appear in the Black-Scholes PDE.

Moreover, and most importantly, the PDE (3.16) splits the differential operator in the PDE (3.7). This is the cornerstone of the numerical scheme here proposed.

We use a characteristics (or semi-Lagrangian) scheme to discretize in time the term of the total derivative. This is, again, common in fluid dynamics and other convection-dominated problems (Douglas and Russell, 1982). In such cases, the characteristic lines are the trajectories followed by fluid particles as they move through a flow field. These lines are solutions to the Ordinary Differential Equations (ODEs) that describe the motion of individual fluid particles. So, we perform a finite difference discretization of the time derivative along the characteristic lines, as in Baamonde-Seoane et al. (2021) and detailed in Douglas and Russell (1982).

To do so, we set a total number of time points $N_T > 0$ and a time step $\Delta\tau = \gamma/N_T$. Thus, we have a uniform time mesh $\{\tau^n = n\Delta\tau\}, n = 0, 1, \ldots, N_T$. At each time step, we know the trajectory $\chi(s)$ of a particle subject to the velocity field v through the point $(\tau^{n+1}, \hat{B})$ must satisfy the initial value ODE

$$\frac{\mathrm{d}\chi}{\mathrm{d}s}(s) = -\frac{1}{\hat{b}}\exp\left(\hat{G}\hat{g} - \bar{g}\right), \quad \chi(\tau^{n+1}) = \hat{B}. \tag{3.17}$$

The solution to this problem is exact and known:

$$\chi(s) = \hat{B} + \frac{1}{\hat{b}}(\tau^{n+1} - s)\exp\left(\hat{G}\hat{g} - \bar{g}\right). \tag{3.18}$$

Let $\chi^n = \chi(\tau^n)$ be the position at the time node τ^n of the point placed at $\left(\hat{B}, \hat{G}\right)$ at time τ^{n+1} and moving according to the velocity field v. Then,

$$\chi^n(\hat{B}, \hat{G}) = \hat{B} + \frac{\Delta\tau}{\hat{b}}\exp\left(\hat{G}\hat{g} - \bar{g}\right). \tag{3.19}$$

Again, we highlight that this position is invariant in the direction $\hat{G}$, because the velocity field is in the direction $\hat{B}$ only. So, we can approximate the total derivative:

$$\frac{DP}{D\tau}\left(\tau^{n+1}, \hat{B}, \hat{G}\right) \approx \frac{P\left(\tau^{n+1}, \hat{B}, \hat{G}\right) - P\left(\tau^n, \chi^n(\hat{B}, \hat{G}), \hat{G}\right)}{\Delta\tau}. \tag{3.20}$$

For the differential operator $\mathcal{A}P$ term, we use a Crank-Nicolson scheme, which is a very popular numerical scheme in quantitative finance (see, for example, Duffy (2006)). After applying it, the following equation is obtained:

$$\begin{aligned}
&\frac{P^{n+1} - P^n \circ \chi^n}{\Delta\tau} - \frac{\sigma_g^2}{4\hat{g}^2}\left[\frac{\partial^2 P^{n+1}}{\partial \hat{G}^2} + \frac{\partial^2 \left(P^n \circ \chi^n\right)}{\partial \hat{G}^2}\right] \\
&- \frac{\alpha_g}{2\hat{g}}\left(f(T-\tau^{n+1}) - (\hat{G}\hat{g} - \bar{g}) + \frac{\beta_g \omega}{2\alpha_g}\right)\frac{\partial P^{n+1}}{\partial \hat{G}} \\
&- \frac{\alpha_g}{2\hat{g}}\left(f(T-\tau^{n}) - (\hat{G}\hat{g} - \bar{g}) + \frac{\beta_g \omega}{2\alpha_g}\right)\frac{\partial \left(P^n \circ \chi^n\right)}{\partial \hat{G}} \\
&+ \frac{r}{2}\left[P^{n+1} + \left(P^n \circ \chi^n\right)\right] = \frac{\beta_g}{4\hat{g}}\left[\frac{\partial \theta^{n+1}}{\partial \hat{G}} + \frac{\partial \theta^n}{\partial \hat{G}}\right].
\end{aligned} \tag{3.21}$$

To simplify the notation, we have denoted $P\left(\tau^n, \chi^n(\hat{B}, \hat{G}), \hat{G}\right)$ as $P^n \circ \chi^n$.

Notice that we have still not carried out the discretization of the variables $\hat{B}$ and $\hat{G}$. That is crucial to describe the fully discretized algorithm, but also to compute the terms $P^n \circ \chi^n$ in (3.21).

Analogously to the time mesh, we introduce uniform finite differences spatial meshes. Let $N_{\hat{B}}$ and $N_{\hat{G}}$ be the number of spatial steps in directions $\hat{B}$ and $\hat{G}$, respectively. Moreover, let $\Delta\hat{B}$ and $\Delta\hat{G}$ be the spatial steps corresponding to those variables. Recalling that the domain where the PDE (3.16) is defined is $\widetilde{\Omega}$, we have $\Delta\hat{B} = {}^1/_{N_{\hat{B}}}$ and $\Delta\hat{G} = {}^1/_{N_{\hat{G}}}$. So, a generic node of the time-space mesh is represented as $(\tau^n, \hat{B}_i, \hat{G}_j) = (n\Delta\tau, i\Delta\hat{B}, j\Delta\hat{G})$ for indices $n = 0, 1, \ldots, N_T$, $i = 0, 1, \ldots, N_{\hat{B}}$ and $j = 0, 1, \ldots, N_{\hat{G}}$.

By (3.20), it is clear that $P^n \circ \chi^n$ must be evaluated at each time step. Unlike Baamonde-Seoane et al. (2021), who use biquadratic interpolation, we compute those terms using a linear interpolation from price values at the finite-difference mesh points, as in Vázquez (1998). This is done mainly for simplicity and consistency reasons. First, since the velocity field v is only in the direction $\hat{B}$, a biquadratic interpolation would degenerate into a quadratic interpolation, as the trajectory of a point starting at mesh node $(\tau^n, \hat{B}_i, \hat{G}_j)$ would only suffer changes in the second coordinate. Secondly, a quadratic interpolation formula requires three mesh points for estimation purposes, so near the edge of our domain, its accuracy could be compromised. A linear interpolation is not as sophisticated, but ensures the same accuracy on the entire domain.

Because the velocity field is one-dimensional, $P\left(\tau^n, \chi^n(\hat{B}_i, \hat{G}_j), \hat{G}_j\right)$ is located in the same line in the direction $\hat{B}$ which passes, namely, by the mesh points $P(\tau^n, \hat{B}_i, \hat{G}_j)$ and $P(\tau^n, \hat{B}_{i+1}, \hat{G}_j)$. So, as Vázquez (1998), we will introduce a restriction (whose derivation is in the Appendix) for the time step that implies that $\hat{B}_i < \chi^n(\hat{B}_i, \hat{G}_j) < \hat{B}_{i+1}$ for all appropriate values of i and j, which is:

$$\Delta\tau < e^{-\bar{g}}\hat{b} \cdot \Delta\hat{B}. \tag{3.22}$$

This way, we can consider the linear approximation for all appropriate values of i and j,

$$P\left(\tau^n, \chi^n(\hat{B}_i, \hat{G}_j), \hat{G}_j\right) \approx \alpha_{i,j} P\left(\tau^n, \hat{B}_i, \hat{G}_j\right) + (1-\alpha_{i,j}) P\left(\tau^n, \hat{B}_{i+1}, \hat{G}_j\right), \tag{3.23}$$

with

$$\alpha_{i,j} = \frac{\hat{B}_{i+1} - \chi^n\left(\hat{B}_i, \hat{G}_j\right)}{\Delta\hat{B}}. \tag{3.24}$$

Using central differences to numerically compute the derivatives in (3.21), one arrives at the full discretization of that problem, for each and all appropriate values of n, i, and j,

$$\begin{aligned}
&\frac{P^{n+1}_{i,j} - \alpha_{i,j}P^n_{i,j} + (1-\alpha_{i,j})P^n_{i+1,j}}{\Delta\tau} + \frac{r}{2}\left[P^{n+1}_{i,j} + \alpha_{i,j}P^n_{i,j} + (1-\alpha_{i,j})P^n_{i+1,j}\right] \\
&- \frac{\sigma_g^2}{4\hat{g}^2}\left[\frac{\begin{array}{l}P^{n+1}_{i,j+1} - 2P^{n+1}_{i,j} + P^{n+1}_{i,j-1} + \alpha_{i,j+1}P^n_{i,j+1} + (1-\alpha_{i,j+1})P^n_{i+1,j+1} \\ \quad - 2\left(\alpha_{i,j}P^n_{i,j} + (1-\alpha_{i,j})P^n_{i+1,j}\right) + \alpha_{i,j-1}P^n_{i,j-1} + (1-\alpha_{i,j-1})P^n_{i+1,j-1}\end{array}}{\left(\Delta\hat{G}\right)^2}\right] \\
&- \frac{\alpha_g}{4\hat{g}}\left(f(T-\tau^{n+1}) - (\hat{G}\hat{g} - \bar{g}) + \frac{\beta_g\omega}{2\alpha_g}\right)\left[\frac{P^{n+1}_{i,j+1} - P^{n+1}_{i,j-1}}{\Delta\hat{G}}\right] \\
&- \frac{\alpha_g}{4\hat{g}}\left(f(T-\tau^{n}) - (\hat{G}\hat{g} - \bar{g}) + \frac{\beta_g\omega}{2\alpha_g}\right)\left[\frac{\begin{array}{l}\alpha_{i,j+1}P^n_{i,j+1} + (1-\alpha_{i,j+1})P^n_{i+1,j+1} \\ \quad - \alpha_{i,j-1}P^n_{i,j-1} + (1-\alpha_{i,j-1})P^n_{i+1,j-1}\end{array}}{\Delta\hat{G}}\right] \\
&- \frac{\beta_g}{8\hat{g}}\left[\frac{\theta^{n+1}_{i,j+1} - \theta^{n+1}_{i,j-1} + \theta^n_{i,j+1} - \theta^n_{i,j-1}}{\Delta\hat{G}}\right] = 0,
\end{aligned} \tag{3.25}$$

where we simplified the notation for the approximations at the mesh nodes $P^l_{r,s} \approx P\left(\tau^l, \hat{B}_r, \hat{G}_s\right)$ and $\theta^l_{r,s} \approx \theta\left(\tau^l, \hat{B}_r, \hat{G}_s\right)$.

We remember that (3.25) is coupled with the nonlinear relation between P and θ described in (3.8) at each time step, i.e.,

$$\theta^{n+1} = m^\omega_\lambda\left(P^{n+1} + \lambda\theta^{n+1}\right). \tag{3.26}$$

So, in the following subchapter we use a fixed point algorithm first presented in Baamonde-Seoane et al. (2021) to solve this system of equations.

3.3.2 The Subsequent Fixed Point Algorithm

A fixed point algorithm is suitable for this problem because we are dealing with a nonlinear system of two equations with two unknowns: at each time step, we must compute P^{n+1} and θ^{n+1}. The algorithm must first solve equation (3.25) to obtain P^{n+1} for a previously computed value of θ^{n+1}; next, it must update θ^{n+1} as disclosed in (3.26) with the more recent value of P^{n+1}. This process must be iterated until a certain stopping criterion is fulfilled. Hence, we add a superscript to the unknowns: $P^{n+1,k}$ and $\theta^{n+1,k}$ represent the k^{th} iteration of the respective variables.

The algorithm, based on Baamonde-Seoane et al. (2021), is sketched as follows:

Step 1 *Initialize the variables*

$n, k \geq 0$, P^0 and θ^0 initialized (for example, $P^0 = \theta^0 = 1$). [1]

Step 2 *At each time step, solve the linear system, update θ and check the stopping test*

For $n = 0, 1, \ldots, N_T - 1$:

(a) *Initialize θ^{n+1} for the first iteration*

Let $\theta^{n+1,0} = \theta^n$.

(b) *Start the fixed point iterations*

For $k = 0, 1, 2, \ldots$

i. For a given $\theta^{n+1,k}$, we can obtain $P^{n+1,k+1}$ by solving the linear system $\mathcal{C}(\hat{G})P^{n+1,k+1} = b^n$. This system has $(N_{\hat{B}} - 1) \times (N_{\hat{G}} - 1)$ unknowns. If we order the finite differences mesh nodes in lexicographical order, the matrix $\mathcal{C}(\hat{G})$ is block diagonal. It has $N_{\hat{B}} - 1$ blocks of tridiagonal matrices of order $N_{\hat{G}} - 1$ each. Each one of those matrices is given by:

$$\begin{pmatrix} c_1(\hat{G}_1) & c_2(\hat{G}_1) & 0 & \ldots & 0 \\ c_3(\hat{G}_1) & c_1(\hat{G}_1) & c_2(\hat{G}_1) & \ddots & \vdots \\ 0 & \ddots & \ddots & \ddots & 0 \\ \vdots & \ddots & \ddots & c_1(\hat{G}_{N_{\hat{G}}-2}) & c_2(\hat{G}_{N_{\hat{G}}-2}) \\ 0 & \ldots & 0 & c_3(\hat{G}_{N_{\hat{G}}-1}) & c_1(\hat{G}_{N_{\hat{G}}-1}) \end{pmatrix}$$

[1] At this point, we do not have any reasons to believe the variables should be initialized in a different way. Nonetheless, we will comment on how this initialization can be different and more efficient in the subsequent Chapter.

with:

$$c_1(\hat{G}_j) = \frac{1}{\Delta\tau} + \frac{r}{2} + \frac{\sigma_g^2}{2\hat{g}^2\left(\Delta\hat{G}\right)^2},$$

$$c_2(\hat{G}_j) = -\frac{\sigma_g^2}{4\hat{g}^2\left(\Delta\hat{G}\right)^2} - \frac{\alpha_g}{4\hat{g}\left(\Delta\hat{G}\right)}\left(f(T-\tau^{n+1}) - (\hat{G}_j\hat{g} - \bar{g}) + \frac{\beta_g\omega}{2\alpha_g}\right),$$

$$c_3(\hat{G}_j) = -\frac{\sigma_g^2}{4\hat{g}^2\left(\Delta\hat{G}\right)^2} + \frac{\alpha_g}{4\hat{g}\left(\Delta\hat{G}\right)}\left(f(T-\tau^{n+1}) - (\hat{G}_j\hat{g} - \bar{g}) + \frac{\beta_g\omega}{2\alpha_g}\right).$$

Moreover, computationally, $P^{n+1,k+1}$ is the vector that contains the approximation at the k^{th} iteration of the solution at the finite differences mesh nodes by lexicographical order.

On the right-hand side of the linear system, computationally we have a vector $b^n = \left((b^n_{i=1,j}), (b^n_{i=2,j}), \ldots, (b^n_{i=N_{\hat{B}}-1,j})\right)$. for $j = 1, \ldots, N_{\hat{G}} - 1$. For each one of the appropriate values of i and j and at each time step, its components are:

$$\begin{aligned}
\left(b^n_{i,j}\right) =& \frac{\alpha_{i,j}P^n_{i,j} + (1-\alpha_{i,j})P^n_{i+1,j}}{\Delta\tau} + \frac{r}{2}\left[\alpha_{i,j}P^n_{i,j} + (1-\alpha_{i,j})P^n_{i+1,j}\right] \\
&- \frac{\sigma_g^2}{4\hat{g}^2\left(\Delta\hat{G}\right)^2}\Big[\alpha_{i,j+1}P^n_{i,j+1} + (1-\alpha_{i,j+1})P^n_{i+1,j+1} + \alpha_{i,j-1}P^n_{i,j-1} \\
&\qquad - 2\left(\alpha_{i,j}P^n_{i,j} + (1-\alpha_{i,j})P^n_{i+1,j}\right) + (1-\alpha_{i,j-1})P^n_{i+1,j-1}\Big] \\
&- \frac{\alpha_g}{4\hat{g}\Delta\hat{G}}\left(f(T-\tau^n) - (\hat{G}\hat{g} - \bar{g}) + \frac{\beta_g\omega}{2\alpha_g}\right)\Big[\alpha_{i,j+1}P^n_{i,j+1} \\
&\qquad + (1-\alpha_{i,j+1})P^n_{i+1,j+1} - \alpha_{i,j-1}P^n_{i,j-1} + (1-\alpha_{i,j-1})P^n_{i+1,j-1}\Big] \\
&- \frac{\beta_g}{8\hat{g}\left(\Delta\hat{G}\right)}\left[\theta^{n+1}_{i,j+1} - \theta^{n+1}_{i,j-1} + \theta^n_{i,j+1} - \theta^n_{i,j-1}\right] = 0,
\end{aligned}$$

ii. After computing $P^{n+1,k+1}$, update $\theta^{n+1,k+1}$ with the identity stated in (3.26):

$$\theta^{n+1,k+1} = m^{\omega}_{\lambda}\left(P^{n+1,k+1} + \lambda\theta^{n+1,k}\right)$$

Notice that $\theta^{n+1,k+1}$ has the same shape as $P^{n+1,k+1}$: computationally, it is a vector with size $(N_{\hat{B}} - 1) \times (N_{\hat{G}} - 1)$ ordered in lexicographical order.

iii. Defining a small enough $\epsilon > 0$ and using the infinity norm, check the stopping test:

$$\frac{\left\|\theta^{n+1,k+1} - \theta^{n+1,k}\right\|_\infty}{\left\|\theta^{n+1,k+1}\right\|_\infty} < \epsilon$$

(c) If the stopping test is satisfied, then restart **Step 2** with the next time step; otherwise, go to (b).

An important note about the algorithm above is that it does not include the imposition of Neumann boundary conditions mentioned in a previous subchapter in (3.13). In the next Chapter, it will be shown that this numerical method and its implementation will be tested in a so-called "academic test", i.e., in a PDE with a known analytical solution. For that reason, in that test we do not impose Neumann boundary conditions. Instead, we set Dirichlet boundary conditions that are given by evaluating the known analytical solution at the corresponding boundaries, as in Baamonde-Seoane et al. (2021). Only after this test, the algorithm is utilized in a real case, in which Neumann boundary conditions are imposed. Therefore, to ensure that the algorithm above is a sketch that is adequate for both cases, we do not address the issue of boundary conditions. However, we indicate that we impose such conditions by adding them directly to the solution at each time step. This is performed by adding two lines and two columns to each of the tridiagonal matrices that make up the block diagonal matrix $\mathcal{C}(\hat{G})$ and the corresponding entries to the vectors P^{n+1} and θ^{n+1}. Then, we impose the desired spatial boundary conditions appropriately. As for the boundary condition referent to compliance dates, it is done directly in the price vector P.

Chapter 4

Results and Discussion

In this Chapter we present and discuss some numerical results after implementing the pricing model. First, we check the performance of the proposed numerical method and then we focus on a real world scenario, as in Baamonde-Seoane et al. (2021). Last but not least, we see how the model reacts to changes in the feedback parameter via a sensitivity analysis, based on the paper by Coulon et al. (2015).

4.1 Academic Test

We start by running the code we built in *Python* to implement the numerical method in a so-called "academic test", i.e., an example with a known analytical solution. This is an important exercise not only to test whether the implementation was performed correctly but also to check the convergence of the numerical method.

To do so, we use the same non-homogenous PDE as Baamonde-Seoane et al. (2021):

$$\mathcal{L}_1[P] = h, \tag{4.1}$$

where the operator $\mathcal{L}_1$ is the one defined in (2.8) and h is given by

$$\begin{aligned} h(t,B,\widetilde{G}) = \exp\left((T-t)B\widetilde{G}\right)\Bigg[&- B\widetilde{G} + \frac{1}{2}\sigma_g^2(T-t)^2B^2 - \\ &- (T-t)B\alpha_g\left(f(t) + \frac{\beta_g}{\alpha_g}\exp\left((T-t)B\widetilde{G}\right) - \widetilde{G}\right) - \exp\left(\widetilde{G}\right)(T-t)\widetilde{G} - r\Bigg]. \end{aligned} \tag{4.2}$$

This way, $P(t,B,\widetilde{G}) = \exp\left((T-t)B\widetilde{G}\right)$ is the analytical solution of (4.1).

We also consider the single period case ($\gamma = 1$), with $T = 1$. Moreover, once this is a purely academic test, we can choose for the domain truncation the values $\hat{b} = \hat{g} = 1$, and so the PDE problem is posed in the domain $\widetilde{\Omega} = [0, 1]^3$. We do not include the seasonality effect in this test, and so we take $f = 0$. The remaining parameters in the PDE (4.1) are presented in Table 4.1 and taken from Baamonde-Seoane et al. (2021) and Coulon et al. (2015).

Table 4.1: Parameters in the PDE for the academic test.

Parameter	T	γ	α_g	β_g	σ_g	r
Value	1	1	2	1.27×10^{-3}	0.1863	0.02

As for boundary conditions, we impose Dirichlet boundary conditions on $\Gamma_1^{*,+}$, $\Gamma_2^{*,-}$ and $\Gamma_2^{*,+}$, and also the terminal condition at time $t = T$ by evaluating the analytical solution at the corresponding boundaries.

Following Baamonde-Seoane et al. (2021), we take the parameter $\omega = 2$ for the numerical method and $\epsilon = 10^{-5}$ for the stopping criterion. Like the authors, to assess the performance of the numerical method we consider a constant relation between spatial and time steps, but it must check the inequality (3.22).

To ascertain the error when approximating the analytical solution by using the numerical method, we use the infinity norm at each time step n to compute the relative error between the exact and numerical solutions

$$\upsilon_n^{\infty}(\Delta\tau) = \frac{\max\limits_{i,j} \left| P\left(\tau^n, \hat{B}_i, \hat{G}_j\right) - P_{i,j}^n \right|}{\max\limits_{i,j} \left| P\left(\tau^n, \hat{B}_i, \hat{G}_j\right) \right|}, \tag{4.3}$$

and next, we take the maximum of the errors defined for each time step in (4.3):

$$\Upsilon^{\infty}(\Delta\tau) = \max_n \left(\upsilon_n^{\infty}(\Delta\tau)\right). \tag{4.4}$$

For each step size $\Delta\tau$, the radius of convergence is

$$R(\Delta\tau) = \frac{\Upsilon^{\infty}(\Delta\tau)}{\Upsilon^{\infty}(\Delta\tau/2)}, \tag{4.5}$$

and the empirical order of convergence is given by $\log_2(R)$.

Table 4.2: Relative errors and order of convergence.

Time Steps	**Space Steps**	$\boldsymbol{\Upsilon^{\infty}(\Delta\tau)}$	$\boldsymbol{R(\Delta\tau)}$	**Order**
30	16	0.028153	-	-
60	32	0.014045	2.0045	1.0032
120	64	0.007251	1.9370	0.9538
240	128	0.003619	2.0036	1.0026

The results obtained after implementing the numerical method are summarized in Table 4.2.

We note that these results are very similar to those obtained in Baamonde-Seoane et al. (2021). In fact, the small differences that can be reported in terms of relative errors may be due to the fact that we used a linear interpolation to approximate the values $P\left(\tau^n, \chi^n(\hat{B}, \hat{G}), \hat{G}\right)$, while the authors used a quadratic interpolation formula. We also note that our script takes more time to run; in a laptop whose CPU is a Intel(R) Core(TM) i7-7500U @ 2.70GHz with 12GB of RAM, the last row of this academic test took approximately 30 minutes to conclude. In spite of its simplicity, *Python* is notoriously slower at numerical computations and simulations than *MATLAB* (see, for example, Guedes and Nepomuceno (2019)), which was the programming language of choice in Baamonde-Seoane et al. (2021). Besides, in that study, the CPU and RAM units were more powerful.

However, most importantly, we report that a first order convergence is achieved as in Baamonde-Seoane et al. (2021).

4.2 Real Case

In this case, we also follow the work of Baamonde-Seoane et al. (2021) and analyse the evolution of REC prices in a real world scenario. That scenario is the one featured in Coulon et al. (2015) for a particular kind of RECs: the solar renewable energy certificates (SRECs) in the New Jersey market. In that paper, the authors construct a valuation model very similar to the one we presented earlier, calibrate it to the New Jersey market data and backtest it.

Given the similarities between the models, we operate similarly to Baamonde-Seoane et al. (2021) and consider the same parameters that were calibrated in Coulon

et al. (2015). So, we will value RECs with maturity $T = 13$, corresponding to the end of the energy year of 2013, which is May 31, 2013. We also consider the lifespan of the certificate is three years, that is, $\gamma = 3$. That means that the beginning of the certificate is $t_0 = 10$, which corresponds to the date of May 31, 2010. Recall that after changing the time variable, this date is equivalent to $\tau = 3$. The first compliance date is one year after the start of the "life" of the certificate, i.e., May 31, 2011, or equivalently, $\tau = 2$ and $t = 11$.

Some practical information on the model is condensed in Tables 4.3 and 4.4. Table 4.3 encapsulates the parameters considered for the PDE (3.7), including for the seasonality function (2.2), retrieved from Coulon et al. (2015), whereas Table 4.4 showcases the values of the requirement (R_i) and ACP (ACP_i) at the end of each energy year.

Table 4.3: Parameters considered for the PDE in the real test.

Parameter	α_g	β_g	σ_g	r	a_1	a_2	a_3	a_4
Value	2	1.27×10^{-3}	0.1863	0.02	-0.1209	0.0900	0.2151	0.3859

Table 4.4: Requirements and ACPs for each energy year in the real test.

Energy Year	$\boldsymbol{R_i}$	$\textbf{ACP}_i$
2011	306000	675
2012	442000	658
2013	596000	641

As for the parameters that arise from the domain truncation, we choose $\hat{b} = 7 \times 10^5$ and $\bar{g} = \ln(7 \times 10^5)$. This allows to grasp the behaviour of the numerical solution in an appropriate and relevant domain for the values of the stochastic factors.

Regarding the parameters of the discretization, we take the time step $\Delta\tau = 1/400$ and the spatial steps $\Delta\hat{B} = \Delta\hat{G} = 1/32$. As in the academic test, we take the parameter $\omega = 2$ for the duality method and $\varepsilon = 10^{-5}$ for the stopping criterion in the fixed point algorithm.

After implementing and running the script that numerically solves the PDE, we return to the original variables (t, B, G) and plot the numerical results.

As in Baamonde-Seoane et al. (2021), for comparison reasons, out of the entire set of solutions in time we obtained, we choose to present the REC price curves for two moments: eight (Figure 4.1) and four (Figure 4.2) months before maturity.

Figure 4.1: REC price eight months before maturity.

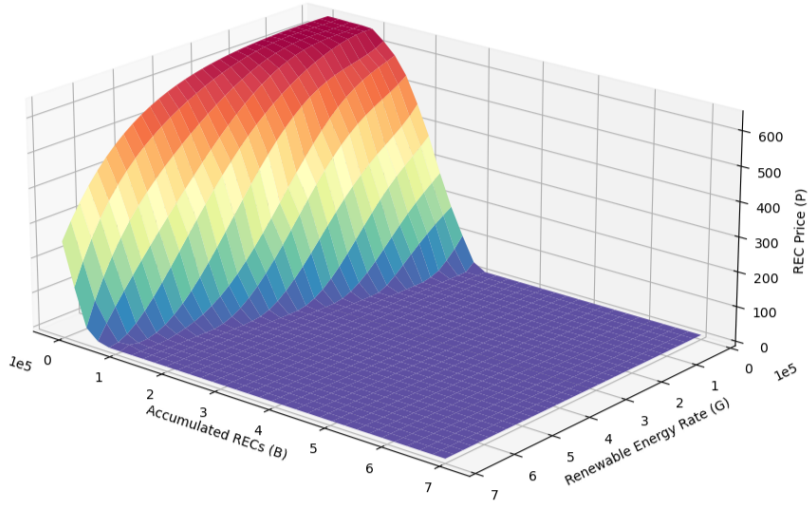

Figure 4.2: REC price four months before maturity.

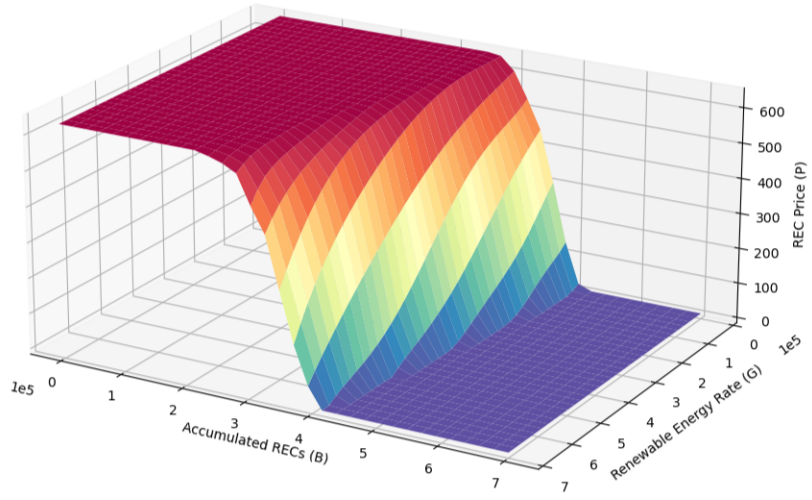

In both cases, the price of the certificate takes values between zero and the value of the ACP, which makes sense economically; in case the LSE fails to comply with regulations, it would be unreasonable to pay a premium for the certificate instead of simply paying for the ACP.

Also, both plots show the inverse relation between the accumulated number of RECs and the price: as supply (B) increases, the price decreases, and vice-versa. Again, this is reasonable, because for a LSE it would make no sense to invest in the purchase of RECs if it already has accumulated a number of them that allows to comply with regulations. That way, the demand drops and so does the price. Conversely, if the number of accumulated RECs does not allow to face regulatory impositions, a LSE's demand for RECs will increase, causing their prices to surge.

Similarly, both plots reveal that REC prices react to changes in the renewable energy generation rate (G). As expected, the greater the renewable energy generation rate, the lower the REC price. This is because a LSE with greater energy generating capability is expected to fulfil the regulatory requirements more easily and so has a lower demand for RECs. Nevertheless, that impact seems to be slightly stronger in Figure 4.1. In that plot, when B approaches zero, the price increases as in Figure 4.2, but a rapid increase is offset by high values of the variable G. In Figure 4.2, a high renewable energy generation rate is not enough by itself to lower the price curve; the REC prices are equal to the ACP amount even for values of accumulated certificates close to the requirement. This is because time before compliance date is running out and energy generation rate has a paramount importance in this period of time.

Furthermore, seeing the figures as a whole, we see the importance of the other factor, which is time to maturity. As we get closer to compliance date, REC prices tend to increase when there are not enough accumulated certificates or when the renewable energy production rate is low. On one hand, this makes sense economically, because in such cases demand increases, which causes the prices to increase as well. On the other hand, it is also important to observe and analyse this fact mathematically. Recall that, at the time of maturity and compliance dates, we have boundary conditions defined by (2.10), which are plotted as three dimensional Heaviside step functions. Furthermore, we solve the PDE backwards in time. So, we conclude that the closer we are to maturity, the more similar the numerical solution is to the maturity boundary condition. As reported in Baamonde-Seoane et al. (2021), the dynamics of the PDE push the cross-sectional curves of REC prices versus the accumulated RECs to the left, which can be also observed in Figures 4.1 and 4.2.

An important note is that the initialization of the price vector in the algorithm proposed in the previous Chapter is not as arbitrary as one would expect. After initializing the vector with the appropriate boundary conditions in time, we initialized the remaining entries of the vector as "transition" states between one boundary and

the next one. These transition states can be thought of as intermediary values that smoothly connect one boundary condition to the next. This construction ensures that our algorithm begins its iterations with a price vector that visually resembles multiple plots, each transitioning gradually from one step function to the next. Without this construction, we observed that our algorithm struggled with slow convergence towards the numerical solution. In some instances, it even triggered another stopping criterion we implemented to prevent excessive computational iterations (specifically, we set a limit of 200 iterations per time step). The root cause of this slow convergence lies in the inherent fixed point nature of our algorithm, as they often heavily depend on the initial solution. By initializing the price vector with these transition states, we mitigate this issue. Our algorithm starts with a price vector that is not too far removed from the expected solution, gradually refining its values over successive iterations. This initialization aligns with the problem's dynamics and assists the algorithm in reaching convergence efficiently.

4.3 Sensitivity Analysis

In the previous subchapter, we analysed the results by observing the price curves in time with respect to the two stochastic factors considered in our work: the accumulated number of renewable energy certificates, and the renewable energy generation rate. However, another exercise that can be done is analysing the sensitivity of the numerical solution of the pricing PDE to changes in its parameters.

Some parameters of the PDE (2.8), such as the ones that control the amplitude of the seasonality function and the volatility of the generation process, are calibrated and backtested in Coulon et al. (2015). The authors have also calibrated the level of feedback, but it is an interesting exercise to see its influence on REC prices, because it may impact investment decisions. The parameter β_g controls how fast new renewable energy production infrastructure is installed when REC prices are high. So, seeing how prices react to different levels of feedback is very relevant economically, because it can help us better understand the dynamics of the renewable energy market and its responsiveness to market conditions.

Moreover, our pricing model features a parameter, α_g, that controls the mean reversion speed of the OU process that drives the renewable energy generation rate, as in Baamonde-Seoane et al. (2021). This parameter is not calibrated by the authors and seems to serve an *ad-hoc* purpose, in spite of its relevance in the model. As it

controls the speed to which the process driving energy generation returns to the mean, its increase should in theory result in a decrease of the volatility in the renewable energy generation process. So, it is also worthwhile to investigate how REC prices are sensitive to changes in this parameter. However, this is a mere mathematical analysis exercise, because market players cannot change this parameter. For an illustration of that, consider an over-simplistic case, for instance in SRECs, where it is possible to plausibly assume that the renewable energy generation rate depends solely on temperature. In that case, a change in the mean reversion speed would simply be a result of changes in weather patterns. Clearly, it is not a tunable parameter by market makers, but rather a characteristic of the market that all participants must be aware of.

To analyse the sensitivity of the model to changes in the parameters α_g and β_g, we start by selecting a set of values for them and then replace them in the implementation of our model. This was done for the feedback parameter, β_g, in Coulon et al. (2015), for the authors' model. Like in that study, we will see how REC average prices and their variability changes with the parameters, as well as the total number of RECs generated. Concerning average prices, our approach is similar to that of the authors. We simply find a numerical solution for the PDE at each time step and take the average of all prices computed. For the first elements in the set of values we considered for α_g and β_g, we normalize the average price obtained to 100 to compare it with the average prices found with the remaining elements of the sets. But since our model has a PDE representation and is not implemented via Monte Carlo simulations like the model in Coulon et al. (2015), we propose another way of measuring price variability instead of standard deviation.

As mentioned before, for each time step we have a three dimensional plot of prices with respect to the two stochastic factors. To measure REC prices' variability, we start by considering the prices at a specific mesh node, at all time points. Intuitively, we proceed by computing the standard deviation of that set of values, again for each mesh node. Next, we calculate the mean of those standard deviations and use this result as an indicator of price variability. Although it is a naive approach because it only encompasses variability for a specific mesh node over time and does not include variations over different mesh nodes at each time step, it serves its purpose as a measure of price fluctuations. In fact, if an outside observer goes to the market, what they see are fluctuations over time, not over two stochastic factors. After computing these variabilities, we act as described for averages prices, normalising the values in a way that the first element is 100 on the scale.

Figure 4.3: The PDE's sensitivity to mean reversion speed and feedback parameters.

(a) Sensitivity to α_g.

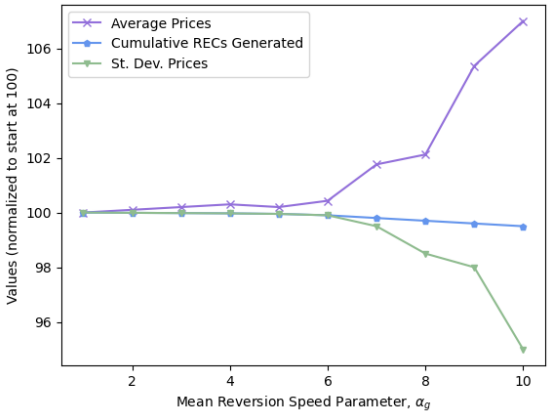

(b) Sensitivity to β_g.

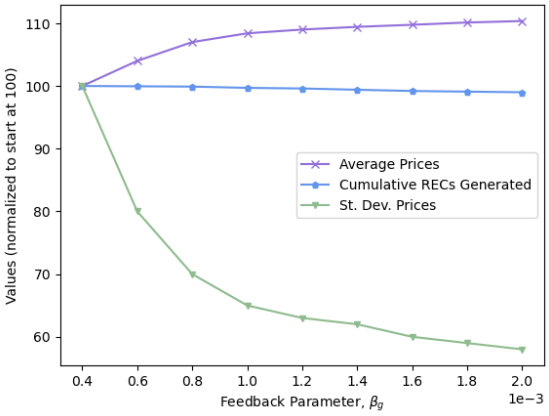

As in Coulon et al. (2015), we also see the impact of changing these parameters in the number of generated RECs. A greater number of accumulated RECs are associated with higher levels of renewable energy being generated, which in turn means that the transition to a greener economy takes place as a faster pace. So, analysing the sensitivity of the PDE to these parameters is interesting for both regulators and market makers. Again, we run our implementation with different values for each parameter and for comparison purposes normalize the values obtained such that the first element of the set of parameters corresponds to 100 on the scale.

The results obtained after deploying this methodology are depicted in Figure 4.3. Note that to arrive to the results in Figure 4.3a, we set β_g with the same value as in the previous subchapter. Analogously, in Figure 4.3b, the mean reversion speed parameter α_g is the same as before.

To properly analyse Figure 4.3a, we first recall that in this thesis and in Baamonde-Seoane et al. (2021) the value considered for the mean reversion speed was $\alpha_g = 2$. Therefore, the first conclusion to be drawn is that there are no major differences in the three measures studied around that value. This can be a reassuring fact: in Baamonde-Seoane et al. (2021), this parameter was not calibrated and is incorporated in the model in an *ad-hoc* way, but between $\alpha_g = 1$ and $\alpha_g = 6$, the numerical solution is similar to the one found with $\alpha_g = 2$. This explains the similarities between our results and the ones in Coulon et al. (2015), where no mean reversion speed parameter is incorporated. It is after $\alpha_g = 6$ that the results start being different. Average prices increase and their variability decreases. This essentially corresponds to a positive shift in the price

axis and a higher resemblance between plots like the ones in Figs. 4.1 and 4.2 at different time instants. However, between $\alpha_g = 1$ and $\alpha_g = 10$, virtually no effects on the number of generated RECs was verified.

Unlike the results of Figure 4.3a, Figure 4.3b expresses some data that can be relevant for decision-makers. The feedback parameter expresses the tendency to invest in renewable energy production technology when REC prices are high, so the higher the feedback parameter, the higher that tendency to respond to REC prices. It is observed that as the feedback parameter increases, the average REC prices increase and their variability decreases by as much as 40%. This is a big revelation for LSEs. Any risk averse individual would be interested in an investment that increases potential profits (average prices can be interpreted as average annual revenues per REC (Coulon et al., 2015)) and decreases risk. So, for such an investor, it would make sense to strongly react to changes in REC prices and install renewable production infrastructure accordingly. Note that this decrease in variability makes sense financially, as installing renewable energy production technology serves as a hedge against changes in REC prices. However, no significant differences in the total number of RECs generated was registered. This is probably due to the nature of REC prices in the domain chosen: a higher feedback parameter is associated to more investment in renewable energy production infrastructure when REC prices are high; when REC prices are low, that urge to invest in such infrastructure is very reduced. Since our domain comprises both scenarios (as seen in Figs. 4.1 and 4.2), they seem to cancel out and overall REC production remains the same.

Chapter 5

Conclusions

The objective of this dissertation was to model the price of renewable energy certificates, following the work of Baamonde-Seoane et al. (2021). The model aims to determine a fair value for any time instant since the start of the certificate's life up to its maturity, depending on two stochastic factors: the renewable energy generation rate and the accumulated number of RECs.

We start by presenting comprehensive models for both stochastic factors. We model the energy production rate as the exponential of an Ornstein-Uhlenbeck process, the classical model for temperature dynamics (Benth et al., 2008). It includes a seasonality function to account for the influence of weather patterns in energy production. The accumulated number of certificates is computed as merely the sum in continuous time of the renewable energy production rate.

Then, we see how compliance requirements univocally determine a certificate's price at compliance time, both in single and in multiple compliance periods. This allows writing a system of coupled forward-backward stochastic differential equations and the associated partial differential equation. The solution of this equation is our certificate's price.

Given the intricacies of that equation, we then delve into the treatment of its non-linear convective term and employ a numerical method that addresses its convection-dominated nature. This was done by using a duality algorithm based on the Yosida approximation of maximal monotone operators, and then by a characteristics scheme in the direction without diffusion and a Crank-Nicolson scheme for the remaining terms. The numerical scheme culminates in a fixed point algorithm.

This algorithm is implemented and then tested in an academic problem with known analytical solution, where it is seen that it converges with order 1. We then consider

a real REC pricing problem for the New Jersey market and arrive at results already known in the literature. Our addition to the state of the art is the sensitivity analysis that is then performed, where we examine the effects of changes in two parameters in certificates' prices. The most relevant result with implications for investors is the impact of an increase in the tendency to install renewable energy production infrastructure when certificate prices are high. When that occurs, average prices (and consequently revenue) increases, and prices' variability decreases. Therefore, any risk-averse investor would be interested in acting accordingly, tending to react when prices are high by installing renewable energy production infrastructure.

The results in this thesis still leave plenty of room for future work. More fundamental research could focus on a result of existence and uniqueness for the derived partial differential equation and for the system of forward-backward stochastic differential equations in (2.7). This last problem is still open because the first forward SDE is coupled with the backward SDE, which is a more complex situation than the ones considered in Bento (2022) and Schwarz (2012). On the more practical front, one could calibrate the model to more recent market data and to different countries. As markets for renewable energy certificates surge all over the world, this may be a very relevant exercise for regulators and investors.

Bibliography

Arregui, I., Cendán, J. J., Parés, C. and Vázquez, C. (2008), 'Numerical solution of a 1-d elastohydrodynamic problem in magnetic storage devices', *ESAIM: Mathematical Modelling and Numerical Analysis* **42**(4), 645–665.
URL: https://doi.org/10.1051/m2an:2008021

Arregui, I., Jesús Cendán, J. and Vázquez, C. (2005), 'A duality method for the compressible Reynolds equation. Application to simulation of read/write processes in magnetic storage devices', *Journal of Computational and Applied Mathematics* **175**(1), 31–40. Selected Papers of the International Conference on Computational Methods in Sciences and Engineering.
URL: https://doi.org/10.1016/j.cam.2004.06.009

Baamonde-Seoane, M. A., del Carmen Calvo-Garrido, M., Coulon, M. and Vázquez, C. (2021), 'Numerical solution of a nonlinear PDE model for pricing Renewable Energy Certificates (RECs)', *Applied Mathematics and Computation* **404**, 126199.
URL: https://doi.org/10.1016/j.amc.2021.126199

Benth, F. E., Benth, J. S. and Koekebakker, S. (2008), *Stochastic Modeling of Electricity and Related Markets*, World Scientific.
URL: https://www.worldscientific.com/doi/abs/10.1142/6811

Bento, A. (2022), Forward Backward Stochastic Differential Equations and Pricing in Emission Markets, Master's thesis, ISEG - Lisbon School of Economics and Management, University of Lisbon.
URL: http://hdl.handle.net/10400.5/26647

Bermúdez, A. and Moreno, C. (1981), 'Duality methods for solving variational inequalities', *Computers & Mathematics with Applications* **7**(1), 43–58.
URL: https://doi.org/10.1016/0898-1221(81)90006-7

Björk, T. (2020), *Arbitrage Theory in Continuous Time*, Oxford University Press.
URL: https://doi.org/10.1093/oso/9780198851615.001.001

Carmona, R., Coulon, M. and Schwarz, D. (2012), 'The valuation of clean spread options: linking electricity, emissions and fuels', *Quantitative Finance* **12**(12), 1951–1965.
URL: https://doi.org/10.1080/14697688.2012.750733

Chassagneux, J.-F., Chotai, H. and Muûls, M. (2017), *A Forward-Backward SDEs Approach to Pricing in Carbon Markets*, Springer.
URL: https://doi.org/10.1007/978-3-319-63115-8

Cockburn, B. and Shu, C.-W. (2001), 'Runge-Kutta Discontinuous Galerkin Methods for Convection-Dominated Problems', *Journal of Scientific Computing* **16**(2), 173–261.
URL: https://doi.org/10.1023/A:1012873910884

Cont, R. and Tankov, P. (2003), *Financial Modelling with Jump Processes*, i edn, Taylor & Francis.
URL: https://doi.org/10.1201/9780203485217

Coulon, M., Khazaei, J. and Powell, W. B. (2015), 'SMART-SREC: A stochastic model of the New Jersey solar renewable energy certificate market', *Journal of Environmental Economics and Management* **73**, 13–31.
URL: https://doi.org/10.1016/j.jeem.2015.05.004

Douglas, Jr., J. and Russell, T. F. (1982), 'Numerical Methods for Convection-Dominated Diffusion Problems Based on Combining the Method of Characteristics with Finite Element or Finite Difference Procedures', *SIAM Journal on Numerical Analysis* **19**(5), 871–885.
URL: https://doi.org/10.1137/0719063

Duffy, D. J. (2006), *Finite Difference Methods in Financial Engineering*, John Wiley & Sons, Ltd.
URL: https://onlinelibrary.wiley.com/doi/abs/10.1002/9781118673447.fmatter

Guedes, P. F. S. and Nepomuceno, E. G. (2019), 'Some remarks on the performance

of Matlab, Python and Octave in simulating dynamical systems'.
URL: https://arxiv.org/abs/1910.06117

Howison, S. and Schwarz, D. (2012), 'Risk-Neutral Pricing of Financial Instruments in Emission Markets: A Structural Approach', *SIAM Journal on Financial Mathematics* **3**(1), 709–739.
URL: https://doi.org/10.1137/100815219

International Energy Agency (2021), 'Key World Energy Statistics 2021', https://www.iea.org/reports/key-world-energy-statistics-2021. Accessed: 2023-03-07.

Øksendal, B. (2003), *Stochastic Differential Equations - An Introduction with Applications*, Universitext, Springer Berlin, Heidelberg.
URL: https://doi.org/10.1007/978-3-642-14394-6

Oleĭnik, O. A. and Radkevič, E. V. (1973), *The First Boundary Value Problem*, Springer US, Boston, MA, pp. 15–113.
URL: https://doi.org/10.1007/978-1-4684-8965-1_2

Schwartz, E. S. (1997), 'The Stochastic Behavior of Commodity Prices: Implications for Valuation and Hedging', *The Journal of Finance* **52**(3), 923–973.
URL: https://doi.org/10.1111/j.1540-6261.1997.tb02721.x

Schwarz, D. (2012), Price Modelling and Asset Valuation in Carbon Emission and Electricity Markets, PhD thesis, University of Oxford.
URL: ora.ox.ac.uk/objects/uuid:7de118d2-a61b-4125-a615-29ff82ac7316

United Nations (1997), 'Kyoto Protocol to the United Nations Framework Convention on Climate Change', https://web.archive.org/web/20181008095709/https://treaties.un.org/pages/ViewDetails.aspx?src=TREATY&mtdsg_no=XXVII-7-a&chapter=27&lang=en. Accessed: 2023-06-14.

United Nations (2022), 'World population to reach 8 billion on 15 November 2022', https://www.un.org/en/desa/world-population-reach-8-billion-15-november-2022. Accessed: 2023-03-07.

Vázquez, C. (1998), 'An upwind numerical approach for an American and European option pricing model', *Applied Mathematics and Computation* **97**(2), 273–286. **URL:** https://doi.org/10.1016/S0096-3003(97)10122-9

World Bank (2023), 'Poverty Calculator', https://pip.worldbank.org/poverty-calculator. Accessed: 2023-03-07.

Appendix

Modelling

Derivation of the Pricing SDE

With a non-negative interest rate, equation (2.5) implies that the price process P_t is bounded with values between 0 and π_T. Therefore, $\mathbb{E}^{\mathbb{Q}}[P_T^2] < \infty$. We construct a filtration $\mathcal{F}_t^{\mathbb{Q}}$ generated by the Brownian motion W_t^0, which is a Wiener process under the measure $\mathbb{Q}$. So, the price process is adapted to the filtration.

Thus, by the Martingale Representation Theorem (see, for example, Øksendal (2003)), there is a unique process Z_t^0 which is $\mathcal{F}_t^{\mathbb{Q}}$-adapted and square integrable such that

$$P_t = \mathbb{E}[P_T] + \int_t^T Z_s^0 \, dW_s^0.$$

We can use the tower property to evaluate the expected value in the previous equation. On the other hand, under the equivalent martingale measure we can also write the price process as a diffusion with drift where the drift coefficient is equal to the risk-free rate, i.e,

$$\mathrm{d}P_t = rP_t \, \mathrm{d}t + Z_t^0 \, \mathrm{d}W_t^0 \, .$$

Combining the two expressions, one arrives at:

$$P_t = \pi_T \mathbb{1}_{[0,R_T)}(B_T) - r \int_t^T P_s \, ds - \int_t^T Z_s^0 \, dW_s^0.$$

Deriving the Pricing PDE Associated to the FBSDE

Recall our assumption that the pricing function P depends on two stochastic factors: the accumulated RECs at time t, B_t, and the renewable energy generation rate at the

same instant, $G_t = \exp\left(\widetilde{G}_t\right)$. Thus, $P = P(t, B_t, \widetilde{G}_t)$.

To get an expression for the dynamics of P with respect to those variables, we can apply Itô's formula (e.g., Øksendal (2003)). By applying it, we get:

$$\begin{aligned} \mathrm{d}P_t &= \frac{\partial P}{\partial t}\,\mathrm{d}t + \frac{\partial P}{\partial B}\,\mathrm{d}B_t + \frac{\partial P}{\partial \widetilde{G}}\,\mathrm{d}\widetilde{G}_t + \frac{1}{2}\frac{\partial^2 P}{\partial \widetilde{G}^2}\left(\mathrm{d}\widetilde{G}_t\right)^2 \\ &= \left(\frac{\partial}{\partial t} + \frac{\sigma_g^2}{2}\frac{\partial^2}{\partial \widetilde{G}^2} + \alpha_g\left(f(t) + \frac{\beta_g}{\alpha_g}P - \widetilde{G}\right)\frac{\partial}{\partial \widetilde{G}} + \exp\left(\widetilde{G}\right)\frac{\partial}{\partial B}\right)P\,\mathrm{d}t + \sigma_g\frac{\partial P}{\partial \widetilde{G}}\,\mathrm{d}W_t^0\,. \end{aligned}$$

On the other hand, under the equivalent martingale measure $\mathbb{Q}$, P_t has a drift equal to the risk-neutral rate, as it can be seen in the last equation of the system (2.7). Therefore, the drift coefficient of the previous equation must be equal to the one in (2.7), which straightforwardly yields the PDE (2.8).

Numerical Methods

Equivalence of Equations (3.6) and (3.12)

This equivalence is derived by a simple usage of the chain rule. Recalling the change of variables introduced in (3.9), we use the chain rule in Leibniz's notation to see that

$$\frac{\partial P}{\partial B} = \frac{\partial P}{\partial \hat{B}}\frac{\mathrm{d}\hat{B}}{\mathrm{d}B} = \frac{1}{\hat{b}}\frac{\partial P}{\partial \hat{B}}.$$

Analogously, the following expressions are derived for the partial derivatives with respect to $\hat{G}$:

$$\frac{\partial P}{\partial \widetilde{G}} = \frac{1}{\hat{g}}\frac{\partial P}{\partial \hat{G}}, \quad \frac{\partial^2 P}{\partial \widetilde{G}^2} = \frac{1}{\hat{g}^2}\frac{\partial^2 P}{\partial \hat{G}^2}.$$

In these new variables (see (3.10)), (3.6) is rewritten using the results above:

$$\mathcal{L}_2[P] = \frac{\partial P}{\partial y_0} + \frac{\sigma_g^2}{2\hat{g}^2}\frac{\partial^2 P}{\partial y_2^2} + \frac{\alpha_g}{\hat{g}}\left(f(y_0) - (y_2\hat{g} - \bar{g}) + \frac{\beta_g\omega}{2\alpha_g}\right)\frac{\partial P}{\partial y_2} + \frac{1}{\hat{b}}\exp(y_2\hat{g} - \bar{g})\frac{\partial P}{\partial y_1} - rP$$

Then, (3.12) expresses this equation in a more condensed manner.

Derivation of the Time Step Restriction

Recall that in Chapter 3 we justify how $P\left(\tau^n, \chi^n(\hat{B}_i, \hat{G}_j), \hat{G}_j\right)$ is located in the same line in the direction $\hat{B}$ which passes, namely, by the mesh points $P\left(\tau^n, \hat{B}_i, \hat{G}_j\right)$

and $P\left(\tau^n, \hat{B}_{i+1}, \hat{G}_j\right)$. We here derive a restriction for the time step that implies that $\hat{B}_i < \chi^n\left(\hat{B}_i, \hat{G}_j\right) < \hat{B}_{i+1}$, following an idea found in Vázquez (1998).

First, as $\Delta\tau, \hat{b} > 0$ and the exponential function is strictly positive, it is clear by (3.19) that $\chi^n\left(\hat{B}_i, \hat{G}_j\right) > \hat{B}_i, \forall i \in \{0, 1, \ldots, N_{\hat{B}}\}, j \in \{0, 1, \ldots, N_{\hat{G}}\}$. Therefore, we need to ensure that

$$\begin{aligned}
&\chi^n\left(\hat{B}_i, \hat{G}_j\right) < \hat{B}_{i+1} = \hat{B}_i + \Delta\hat{B}, && \forall i \in \{0, 1, \ldots, N_{\hat{B}}\}, j \in \{0, 1, \ldots, N_{\hat{G}}\} \\
\iff &\hat{B}_i + \frac{\Delta\tau}{\hat{b}} \exp\left(\hat{G}_j\hat{g} - \bar{g}\right) < \hat{B}_i + \Delta\hat{B}, && \forall i \in \{0, 1, \ldots, N_{\hat{B}}\}, j \in \{0, 1, \ldots, N_{\hat{G}}\} \\
\iff &\Delta\tau < \frac{\hat{b} \cdot \Delta\hat{B}}{\exp\left(\hat{G}_j\hat{g} - \bar{g}\right)}, && \forall j \in \{0, 1, \ldots, N_{\hat{G}}\}
\end{aligned}$$

Recalling that $0 \leq \hat{G} \leq 1$, the sufficient condition for the inequality above to hold for all values of j is

$$\Delta\tau < e^{-\bar{g}}\hat{b} \cdot \Delta\hat{B}.$$